Mapping the electrostatic profiles of cellular membranes

Sharon Eisenberg[a], Ehud Haimov[b,c], Glenn F. W. Walpole[a,d], Jonathan Plumb[a], Michael M. Kozlov[b], and Sergio Grinstein[a,d,e,*]

[a]Program in Cell Biology, Hospital for Sick Children, 686 Bay Street, Toronto, ON, Canada M5G 0A4; [b]Department of Physiology and Pharmacology, Sackler Faculty of Medicine, and [c]Raymond and Beverly Sackler School of Physics and Astronomy, Tel Aviv University, Tel Aviv 6997801, Israel; [d]Department of Biochemistry, University of Toronto, Toronto, ON, Canada M5S 1A8; [e]Keenan Research Centre of the Li Ka Shing Knowledge Institute, St. Michael's Hospital, Toronto, ON, Canada M5C 1N8

ABSTRACT **Anionic phospholipids can confer a net negative charge on biological membranes. This surface charge generates an electric field that serves to recruit extrinsic cationic proteins, can alter the disposition of transmembrane proteins and causes the local accumulation of soluble counterions, altering the local pH and the concentration of physiologically important ions such as calcium. Because the phospholipid compositions of the different organellar membranes vary, their surface charges are similarly expected to diverge. Yet, despite the important functional implications, remarkably little is known about the electrostatic properties of the individual organellar membranes. We therefore designed and implemented approaches to estimate the surface charges of the cytosolic membranes of various organelles in situ in intact cells. Our data indicate that the inner leaflet of the plasma membrane is most negative, with a surface potential of approximately –35 mV, followed by the Golgi complex > lysosomes > mitochondria ≈ peroxisomes > endoplasmic reticulum, in decreasing order.**

Monitoring Editor
Thomas Martin
University of Lausanne

Received: Aug 12, 2019
Revised: Nov 13, 2020
Accepted: Nov 25, 2020

Lipids and (glyco)proteins are the main constituents of biological membranes. Sugar moieties of glycoproteins, glycolipids, and adherent glycocalyx components such as hyaluronic acid can bear ionizable groups that confer a net negative charge on the outer surface of the plasma membrane. The aggregate surface charge of the outer membrane has been estimated indirectly by measuring the ζ potential—the potential at the slipping plane—by electrophoretic means (e.g., Tippe, 1981; Silva Filho *et al.*, 1987) or by measuring streaming potentials (Vandrangi *et al.*, 2012). The plasma membrane, however, is highly asymmetric; its inner (cytosolic) aspect is virtually devoid of carbohydrate moieties. Nevertheless, the cytosolic leaflet is also thought to be negatively charged, due primarily to the accumulation of anionic phospholipids, namely phosphoinositides and phosphatidylserine (PtdSer). Based on biochemical determinations of its lipid composition, the net negative charge of the plasmalemmal inner leaflet is estimated to generate an electrical field of 10^5 V/cm (Olivotto *et al.*, 1996). The membranes of intracellular organelles can also contain anionic lipids, but their precise lipid composition and topology have been difficult to assess and hence their surface charge has not been estimated.

The surface potentials of biological membranes have important functional implications: they can alter the disposition of charged regions of transmembrane proteins, cause local accumulation of soluble counterions in the vicinity—altering the local pH as well as the concentration of physiologically important ions such as calcium—and serve to recruit extrinsic cationic proteins (McLaughlin, 1989). It is therefore important to determine the electrostatic properties of each of the organellar membranes. In principle, this could be accomplished by measuring the ζ potentials of isolated organelles. However, the purity of such preparations is imperfect, changes in lipid composition (particularly phosphoinositide degradation) and sidedness cannot be avoided, and loosely adherent components

This article was published online ahead of print in MBoC in Press (http://www.molbiolcell.org/cgi/doi/10.1091/mbc.E19-08-0436) on December 2, 2020.

*Address correspondence to: Sergio Grinstein (sergio.grinstein@sickkids.ca).

Abbreviations used: FKBP, FK506-binding protein; FRB, FKBP rapamycin-binding; LAMP-1, lysosome-associated membrane protein 1; PM-RFP, palmitoylated-myristoylated-red fluorescent protein; Pre-GFP, prenylated green fluorescent protein; PtdCho, phosphatidylcholine; PtdEth, phosphatidylethanolamine; PtdIns, phosphatidylinositol; PtdSer, phosphatidylserine.

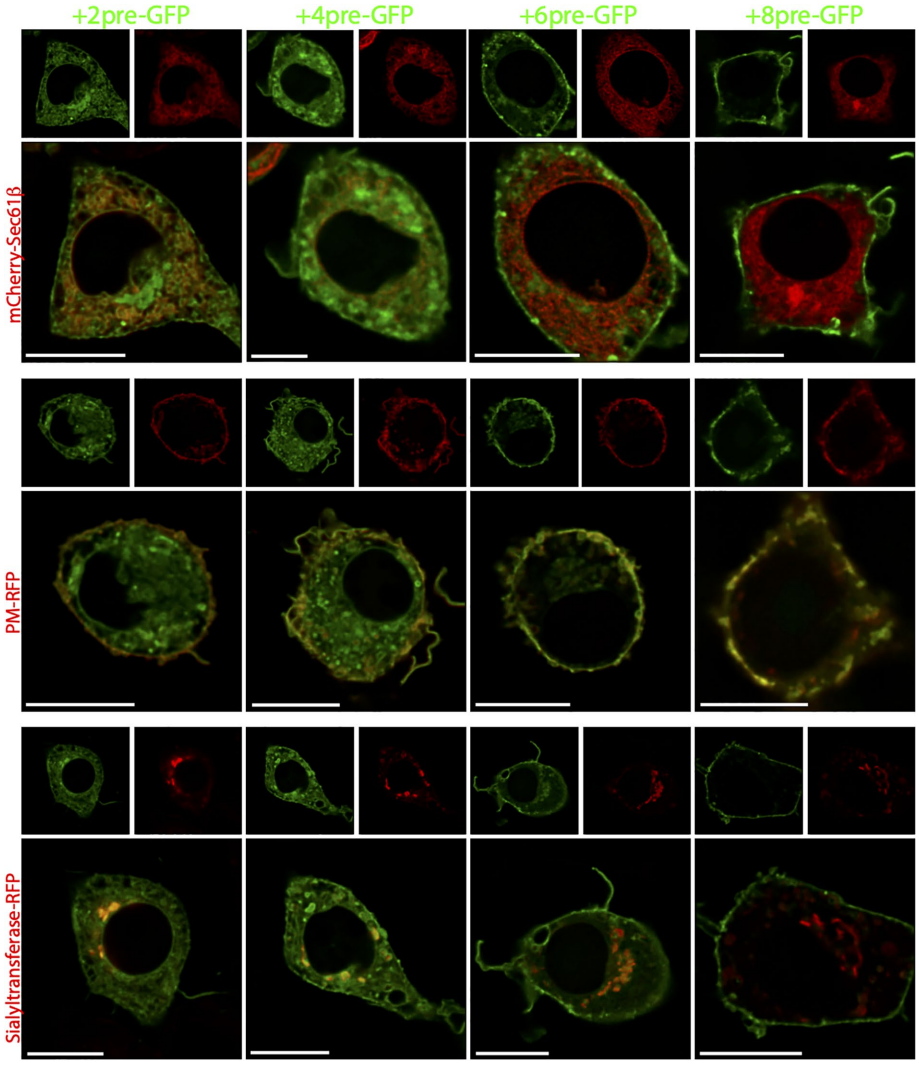

FIGURE 1: Distribution of prenylated charge probes in RAW264.7 cells. Confocal images of RAW264.7 macrophages transiently cotransfected with one of the prenylated surface charge probes (+2-Pre-GFP, leftmost column; +4-Pre-GFP, second column from left; +6-Pre-GFP, third column; +8-Pre-GFP, rightmost column) and an organelle-specific marker (mCherry-Sec61, an ER marker, top row; PM-RFP, a plasmalemmal marker, middle row; sialyltransferase-RFP, a Golgi marker, bottom row). Here and elsewhere, confocal images are representative of at least 20 cells from three different experiments for each condition. The smaller images at the top of each condition show the individual channels (charge probes: green; organellar markers: red), while the main (larger) panels show merged images.

that may alter the surface charge can be removed during the isolation process. Alternative approaches to estimating the surface potential are therefore required.

Here we used recombinant and synthetic polycationic peptides to obtain a quantitative estimate of the surface potential of the inner leaflet of the plasma membrane and to establish a hierarchical map of the potentials of the cytosolic surfaces of the major intracellular organelles in live cells.

RESULTS

We previously reported the use of polycationic peptides to assess the negative nature of the inner leaflet of the plasma membrane (Yeung *et al.*, 2006, 2008). Recombinant peptides tagged with fluorescent proteins were expressed in mammalian cells and their distribution was monitored by confocal microscopy. To avoid association with non-membranous polyanionic structures (primarily nuclear DNA), the peptides were preferentially directed to membranes by inclusion of a hydrophobic determinant, whether in the form of prenylation or by constructing amphiphilic α-helices (Silvius, 1999; Roy *et al.*, 2000; Wright and Philips, 2006; Yeung *et al.*, 2006; Quatela *et al.*, 2008). A similar approach was employed here, but probes of diminishing net charge were constructed, to ensure association with organelles of varying surface potential. These probes were transfected both into RAW264.7 macrophages and into the epithelioid HeLa cells and their distribution was assessed by confocal microscopy by comparison with well-established organellar markers.

As illustrated in Figure 1 (rightmost column), in RAW264.7 cells a prenylated octavalent construct (+8-Pre-GFP) localized almost exclusively to the plasma membrane, identified by coexpression of an RFP-tagged diacylated probe derived from the N-terminal domain of Lyn (termed PM-RFP hereafter). Neither the Golgi complex (identified by expression of tagged sialyltransferase; bottom row) nor the endoplasmic reticulum (identified by expression of tagged Sec61; top row) was discernibly labeled by +8-Pre-GFP. A somewhat less charged prenylated construct (+6-Pre-GFP) associated markedly with the plasma membrane, but also with internal membranes, which included the Golgi (Figure 1; middle column). In contrast, a poorly charged probe (+2-Pre-GFP) bound to virtually all cellular membranes (Figure 1; leftmost column). Essentially identical results were obtained when the prenylated probes and the organellar markers were expressed in HeLa cells (Figure 2).

It is conceivable that the prenyl moiety attached to the probes may have influenced their distribution, directing their partition preferentially to certain membranes depending on the fatty acyl composition of their glycerolipids. To assess this possibility, we performed a similar series of experiments using a second set of probes where the hydrophobic component was provided by the side chains of hydrophobic amino acid residues strategically located on one side of amphiphilic alpha helices. The results are shown in Figures 3 and 4 for RAW264.7 and HeLa cells, respectively. As for the prenylated probes, the results were very similar for both cell types: whereas the +8-helix probe partitioned almost exclusively to the plasmalemma, probes of decreasing charge bound progressively to intracellular organelles. Note that, because the hydrophobicity of the amphiphilic helices is lower than that of the prenylated probes, a considerable fraction of the least charged (+2) helices remained soluble, as indicated by their ability to enter the nuclear space. Collectively, we interpret these data to mean that the most positive probes bind preferentially to the most negatively charged membranes (i.e., the plasmalemma), whereas the partition of poorly

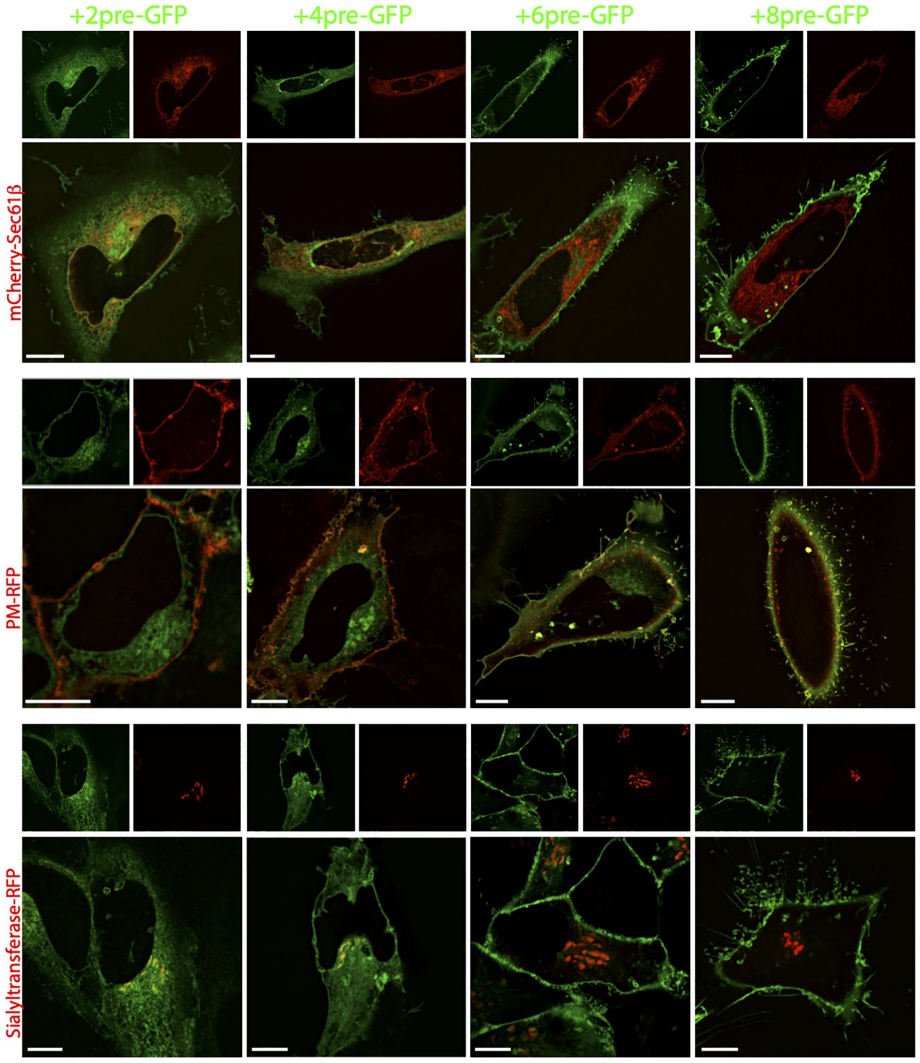

FIGURE 2: Distribution of prenylated charge probes in HeLa cells. Confocal images of HeLa cells transiently cotransfected with one of the prenylated surface charge probes (+2-Pre-GFP, leftmost column; +4-Pre-GFP, second column from left; +6-Pre-GFP, third column; +8-Pre-GFP, rightmost column) and an organelle-specific marker (mCherry-Sec61, an ER marker, top row; PM-RFP, a plasmalemmal marker, middle row; sialyltransferase-RFP, a Golgi marker, bottom row). The smaller images at the top of each condition show the individual channels (charge probes: green; organellar markers: red), while the main (larger) panels show merged images.

charged probes such as +2-Pre-GFP is dictated largely by hydrophobic interactions that are roughly comparable in all cellular membranes. Probes of intermediate charge (e.g., +4-Pre-GFP or +4-Helix-GFP) that are not entirely recruited to the plasma membrane are available for binding to other compartments that are somewhat less negative. Preferential partition of the prenyl group or of the hydrophobic chains of the helix probes into membranes of varying acyl chain composition or lipid packing may have affected their distribution, but the overall similarity of the results obtained with both types of probes lends confidence to the above conclusions, which are also consistent with earlier findings (Yeung *et al.*, 2006, 2008).

Based on the preceding considerations, one can in principle utilize the partition of the various probes to establish an electrostatic hierarchy of the various organellar membranes (note that, because the sensors are expressed in the cytosol and are membrane-impermeant, only the cytosolic aspect of the organellar membranes is probed). However, absolute measurement of the total fluorescence associated with each organelle is not a suitable indication of the binding avidity, as it is affected by the exposed surface area of each organelle, which varies greatly. Therefore, the amount of probe bound must be normalized by the area of each individual organelle. To this end, we quantified the exposed organellar surface using FM4-64, a solvochromic amphiphilic fluorescent dye. Because FM4-64 cannot traverse lipid bilayers, we enabled its access to the cytosolic aspect of organellar membranes (the same surface that is exposed to the surface charge probes) by gently and reversibly permeabilizing the plasma membrane. This was accomplished by transient activation of the purinergic P2 × 7 receptors that are abundant in the membrane of RAW264.7 cells (see diagram in Figure 5A). Exposure of the cells to 5 mM ATP in the absence of divalent cations led to the activation of the receptors, which opens a pore that enables the passage of molecules ≤1000 Da (Dubyak, 2007; Ferreira *et al.*, 2015), including FM4-64 (M_w = 607). Subsequent closure of the pores by removal of ATP and readdition of Mg^{2+} was followed by removal of FM4-64. Because partition of FM4-64 into membranes is readily reversible (Bolte *et al.*, 2004), this ensured that dye associated with the outer leaflet of the plasmalemma would be removed (avoiding overestimation of the area of its inner leaflet) and that only sealed, viable cells were used for the measurements. The effectiveness of this procedure is documented in Figure 5, B–E.

Using the FM4-64 signal to normalize the association of the probes per unit membrane area, we undertook a systematic quantitation of the binding of prenylated probes of +2, +4, +6, and +8 charge to all the major cellular organelles. For this purpose, mitochondria were identified by transfection with Tom70-RFP, peroxisomes with RFP-UBSKL and lysosomes by labeling with LAMP-1. The Golgi complex, endoplasmic reticulum, and plasma membrane were identified as above. The results are summarized in Figure 5F. Briefly, the plasmalemma bound preferentially the most positively charged probes, with proportionally diminishing binding as their charge decreased. Conversely, the endoplasmic reticulum bound a very small amount of the most cationic probe, while binding of the less charged species was progressively more apparent (note that some overlap of the +8 probe with the endoplasmic reticulum was recorded; we believe that this represents regions of the reticulum that abut the plasma membranes, which we cannot resolve using diffraction-limited confocal microscopy). An analogous analysis of the binding pattern of other organelles yielded the following hierarchy: plasma membrane > Golgi complex > lysosomes > mitochondria ≈ peroxisomes > endoplasmic reticulum. We propose that this sequence represents the hierarchy of electronegativity of the cellular organelles.

The preceding results establish the relative order of the surface potentials of various intracellular membranes, but do not provide

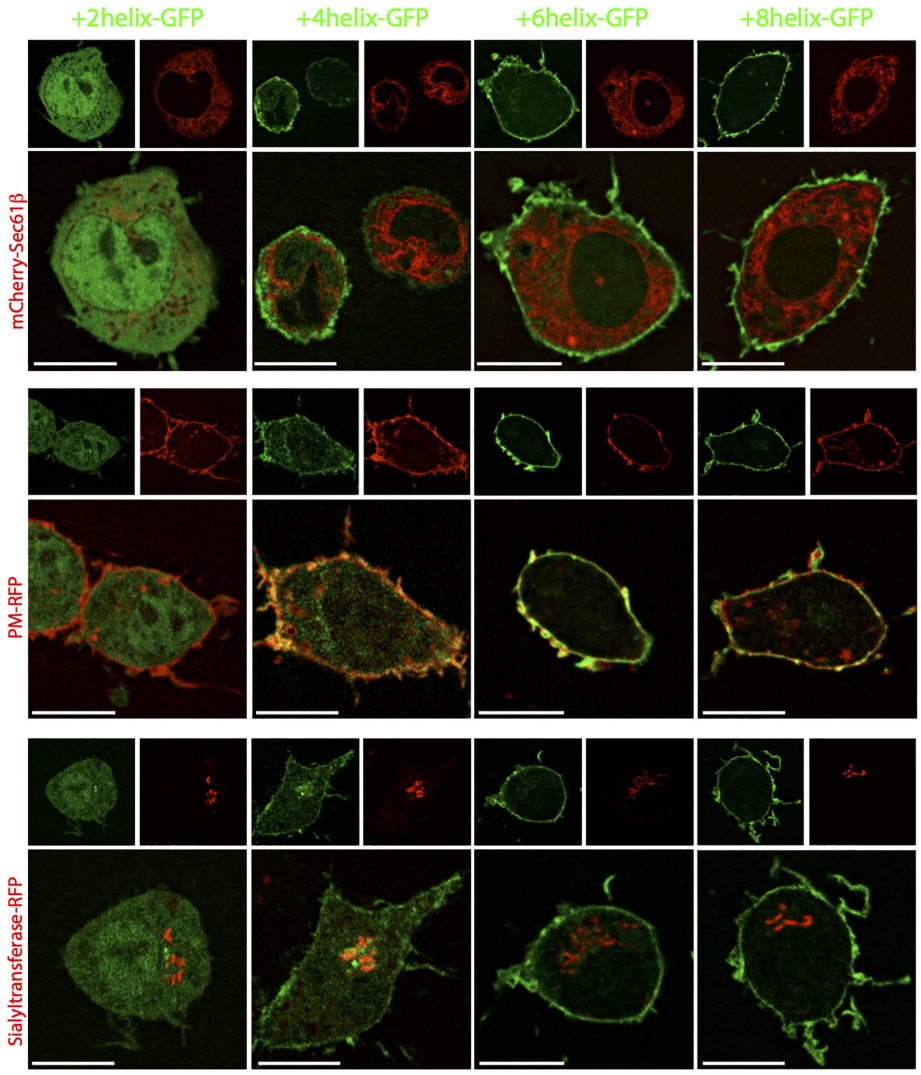

FIGURE 3: Distribution of amphiphilic helical charge probes in RAW264.7 cells. Confocal images of RAW264.7 macrophages transiently cotransfected with one of the surface charge probes (+2-helix-GFP, leftmost column; +4-helix-GFP, second column from left; +6-helix-GFP, third column; +8-helix-GFP, rightmost column) and an organelle-specific marker (mCherry-Sec61, an ER marker, top row; PM-RFP, a plasmalemmal marker, middle row; sialyltransferase-RFP, a Golgi, bottom row). The smaller images at the top of each condition show the individual channels (charge probes: green; organellar markers: red), while the main (larger) panels show merged images.

information of their absolute magnitude. To this end, we sought to quantify a property of the surface potential probes that could be calibrated by comparison with an external standard of known surface or ζ potential. Because the total amount of probe bound to a membrane is proportional not only to the surface potential, but also to its level of expression and to the area of membrane exposed, we measured instead the dissociation rate. This was accomplished using a rapamycin-induced heterodimerization system. Briefly, we constructed a fluorescent surface charge–sensitive probe that also contained a rapamycin-binding FRB domain (see Figure 6A for a diagrammatic representation). In this instance, the charge probes were amphiphilic α-helices, with the hydrophobic contribution provided by leucines and aromatic residues located preferentially on the face of the helix opposed to that displaying the cationic residues. This chimeric probe was transfected into the cells along with a second construct consisting of an FKBP domain targeted to mitochondria by Tom70 and labeled with a different (red) fluorophore. Upon addition of rapamycin, the FRB-containing construct is sequestered on the surfaces of mitochondria at a rate dictated by its dissociation from the negatively charged membrane(s) where it had previously partitioned (Figure 6A). For these experiments, we chose to use HeLa cells, which possess more mitochondria than RAW264.7 cells and can be more reliably cotransfected with appropriate amounts of the two constructs. The effectiveness of this approach is illustrated in Figure 6, B and C, where an octavalent probe normally associated with the plasmalemma was induced to redistribute to the mitochondria by addition of rapamycin. Proper determination of the dissociation rate requires it to be the rate-determining step of the reaction; that is, it is imperative that the entry of rapamycin into the cells and its binding to the FRB and FKBP occur significantly faster. This was validated in two different ways. First, we compared the rate of rapamycin-induced relocalization of the octavalent probe with that for a soluble FRB-containing probe (FLEX-RFP). As shown in Figure 6, D and E, this probe was rapidly recruited to the membrane by a plasmalemmal-associated FKBP-containing probe. Notably, using an identical concentration of rapamycin, the time required for redistribution of the FLEX-RFP probe was much shorter than that required by the octavalent charge probe ($t_{1/2}$ = 11.7 s vs. 42.8 s; Figure 6F). That a tetravalent cationic probe relocalized to mitochondria faster than its octavalent counterpart ($t_{1/2}$ = 19.5 s vs. 42.8 s) is also evidence that entry and binding of rapamycin were not rate-limiting, and is an indication that quantification of the dissociation rate is proportional to—and a suitable measure of—the surface potential. Note that the fraction of the probe displaced from the membrane is dictated by the molar ratio between the FRB- and FKBP-containing components, which are expressed at variable rates. Regardless of the fraction that remains at the membrane, the dissociation rate of the displaced fraction is a reliable indication of the surface potential. We also ensured that availability and binding of intracellular rapamycin would not be rate limiting by analyzing the concentration dependence of the heterodimerizer. As shown in Figure 6G, the time required for recruitment of the octavalent probe did not change when the concentration of rapamycin added to the cells increased between 5 and 20 μM, implying that saturation had been reached at the concentration used for all our experiments (10 μM).

Having determined the rate of dissociation of the helical octavalent probe, we devised means of quantifying the absolute value of the surface potential of the inner leaflet of the plasma membrane. This was accomplished by comparing the dissociation rate determined in vivo with that of an equivalent probe that was allowed to interact with liposomes of defined composition and ζ

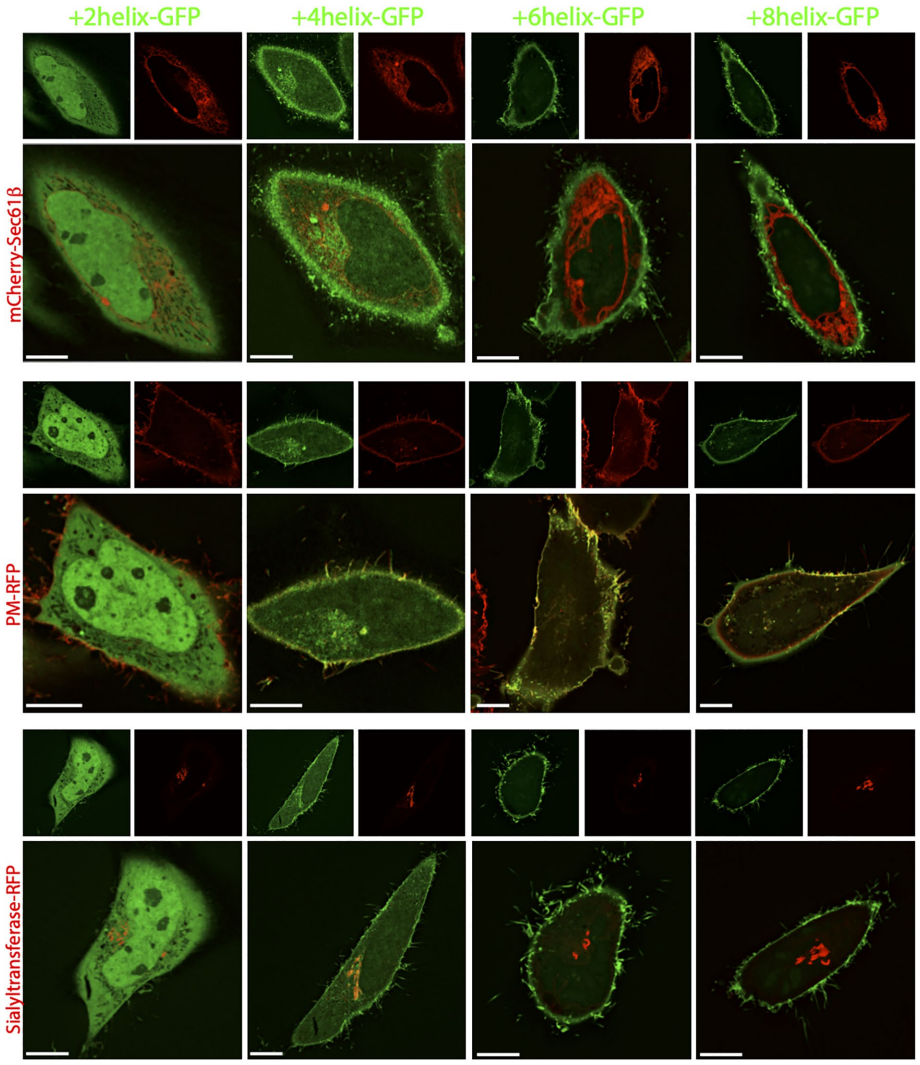

FIGURE 4: Distribution of amphiphilic helical charge probes in HeLa cells. Confocal images of HeLa cells transiently cotransfected with one of the surface charge probes (+2-helix-GFP, leftmost column; +4-helix-GFP, second column from left; +6-helix-GFP, third column; +8-helix-GFP, rightmost column) and an organelle-specific marker (mCherry-Sec61, an ER marker, top row; PM-RFP, a plasmalemmal marker, middle row; sialyltransferase-RFP, a Golgi marker, bottom row). The smaller images at the top of each condition show the individual channels (charge probes: green; organellar markers: red), while the main (larger) panels show merged images.

potential. Giant unilamellar liposomes of varying surface charge were generated by combining PtdCho with increasing amounts (10–30%) of PtdSer. To visualize the liposomes, a small fraction (1%) of rhodamine-labeled PtdEth was also included. In addition, 1% of biotin-conjugated PtdEth was added to the lipid mixture to enable immobilization of the liposomes on avidin-coated coverslips (see diagram in Figure 7A). The immobilized giant liposomes were allowed to bind the fluorescent octavalent probe, and dissociation was initiated by rapid removal of the soluble (unbound) probe, accomplished by perfusing the medium (indicated as "wash" in the diagram of Figure 7A). The dissociation of the probe was then recorded by monitoring the fluorescence that remained associated with the liposomes as time proceeded (Figure 7, B–D).

Liposomes of varying composition—and hence different surface charge density—were used for these experiments, to study the dependence of the dissociation rate on the charge. Note that the lipid compositions of the two monolayers that constitute the membranes of the giant liposomes are identical, unlike those of biological membranes. However, in both instances the surface potential is dictated exclusively by the exofacial monolayer. The surface potential of the liposomes was assessed indirectly, by measuring their ζ potential electrophoretically using the Zetasizer. As expected, the ζ potential became progressively more negative as the PtdSer content of the liposomes increased (Figure 7E). The potentials we measured are consistent with those reported earlier by Roy and colleagues for smaller liposomes of similar composition (Roy *et al.*, 1998). More importantly, the time required for dissociation of the charge probes increased along with the ζ potential (Figure 7F). As anticipated, the dissociation time was considerably longer for the +8 probe than for a probe with only +4 charges; the dependence on the concentration of PtdSer was also steeper for the +8 probe (Figure 7F). Having established the dependence of the dissociation rate of the probe on the ζ potential, we were able to interpolate the potential of the inner leaflet of the plasma membrane of HeLa cells, based on the dissociation rates measured in experiments like those in Figure 6. We estimated this potential to be equivalent to that generating a ζ potential of –35 mV in medium of physiological ionic strength.

Having estimated the absolute magnitude of the potential of the inner surface of the plasmalemma, we attempted to quantify the potential of the organellar membranes also. To this end, we derived equations that enabled us to calculate the differences between the surface potentials of intracellular organelles, based on the measured numbers of the probes bound by each organelle, normalized per unit surface area. These equations, detailed in the Appendix, are based on the notion that, at equilibrium, the probe molecules bound to different membranes must have equal molecular free energy (chemical potential), and assume that the hydrophobic component of the probes partitions similarly in all organellar membranes. As summarized in Table 1, and consistent with the earlier results, we found the plasma membrane to be most negative (–35 mV) and the ER least negative (–14.4 mV), while the Golgi complex and mitochondria displayed intermediate potentials.

DISCUSSION

Electrostatic interactions are thought to be important for the recruitment and retention of proteins by biological membranes, as well as in the establishment of the juxtamembrane ionic concentrations and pH. While these roles are generally acknowledged, little is known about the surface potential of the different intracellular compartments. To address this deficiency, we undertook measurements of the relative surface charge of the major intracellular organelles, using genetically encoded probes tagged with fluorescent proteins. The design of the probes was based conceptually on the structure

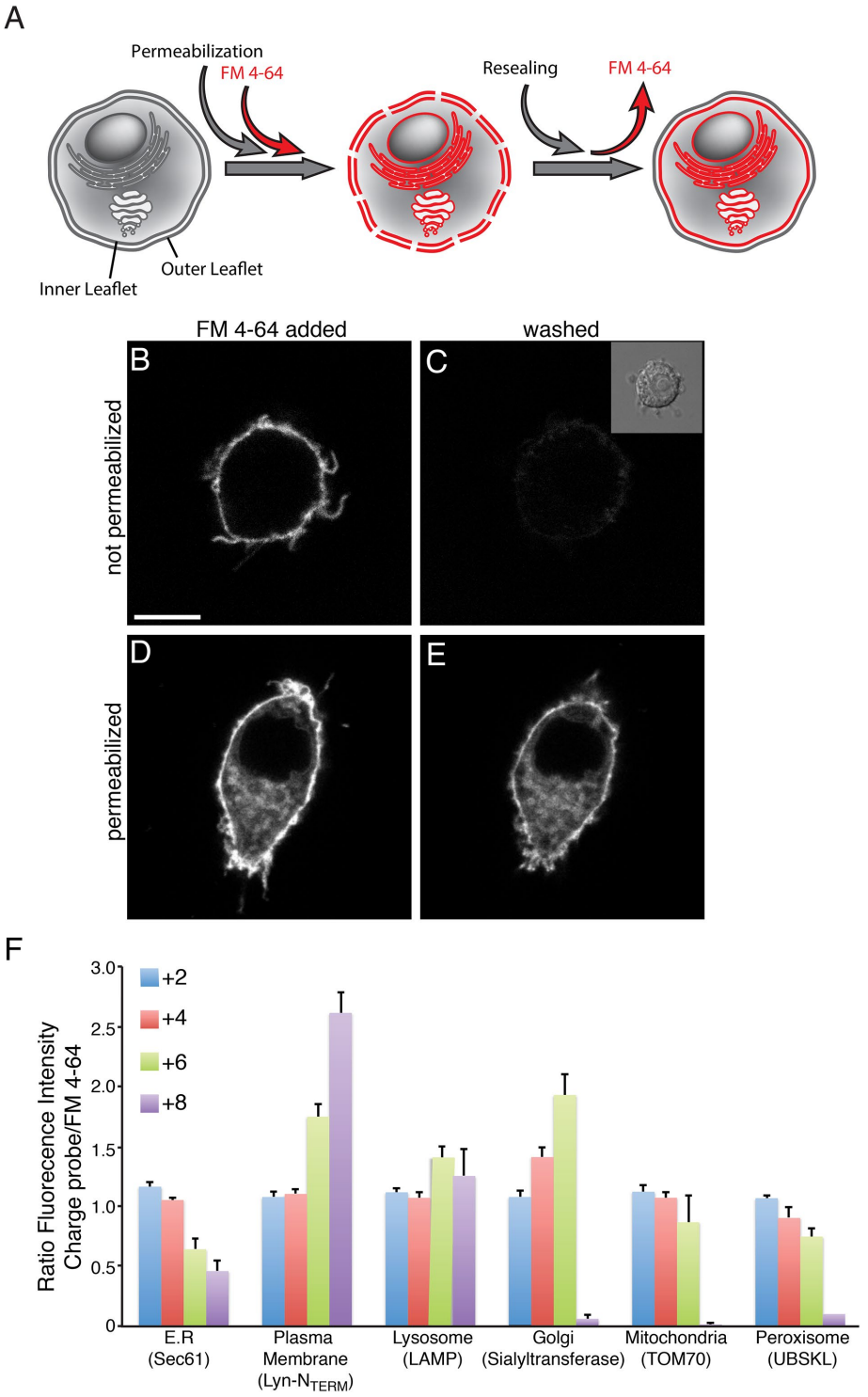

FIGURE 5: Quantification of charge probe distribution in different membrane organelles. (A) Diagrammatic representation of the procedure used to quantify the area of the cytosolic aspect of cellular membranes. Membranes are transiently permeabilized by activation of P_2X_7 receptors with ATP, exposed to the impermeant solvochromic dye FM4-64, and then resealed, followed by removal of extracellular FM4-64. (B, C) Representative confocal images of a RAW264.7 cell incubated with FM 4-64 and acquired in the presence of the dye, B, or after washing, C. (D) Representative confocal image of a RAW264.7 cell that was permeabilized by activating P_2X_7 receptors and labeled with FM 4-64 while permeabilized. (E) The cell shown in D was induced to reseal by removal of ATP and reintroduction of divalent cations while in the presence of FM4-64, followed by washing of the extracellular FM4-64. Images in B–E are representative of at least 20 cells from three different experiments for each condition. (F) Quantification of the ratio of the fluorescence of the charge probes to that of FM4-64. Cells were cotransfected with the indicated charge probe and organellar marker, permeabilized to allow partition of FM4-64 to the cytosolic leaflet of all endomembranes, sealed, and washed to remove extracellular FM4-64, before the fluorescence of all three fluorophores was measured. Results are presented as the fraction of the fluorescence intensity of the probe in each organelle divided by the fraction of the surface area occupied by the organelle (FM4-64 labeling).

of K-Ras, a protein known to be recruited electrostatically to the plasma membrane (Wright and Philips, 2006; Quatela *et al.*, 2008). The carboxy terminus of K-Ras is highly cationic and includes a prenylation site; the combination of these features targets the protein preferentially to highly anionic membrane interfaces (Yeung *et al.*, 2006). In our probes, lysines were replaced by arginines to obviate the possibility of ubiquitination, which could have affected the net charge of the constructs. It is also noteworthy that we obtained similar results using amphiphilic α-helical probes (Figures 3 and 4). The differential distribution of the arginine-rich prenylated probes cannot therefore be attributed to selective partitioning of the prenyl group in membranes of varying fluidity. By comparing the behavior of a series of such cationic probes of diminishing charge, we concluded that the cytosolic aspect of the plasma membrane is the most negative membrane, followed by those of the Golgi complex, lysosomes, mitochondria ≈ peroxisomes, and the endoplasmic reticulum, in decreasing order. This sequence is generally consistent with the known lipid composition of these organelles: the plasmalemma is rich in anionic phospholipids, primarily PtdSer, PtdIns(4)P, and PtdIns(4,5)P_2. The Golgi complex also contains sizable amounts of PtdIns(4)P and significant levels of PtdSer, while late endosomes/lysosomes contain detectable PtdSer and PtdIns(4)P and are the site where PtdIns(3,5)P_2 is thought to be generated (van Meer *et al.*, 2008; Leventis and Grinstein, 2010; Hammond *et al.*, 2014; Hasegawa *et al.*, 2017). On the other hand, the cytosolic leaflet of the endoplasmic reticulum and of peroxisomes appears to consist largely of neutral/zwitterionic lipids, accounting for the inability of these organelles to attract the most cationic probes. As discussed above, the small amount of the +8-Pre-GFP probe assigned as binding to the reticulum likely reflects areas where this organelle forms contacts with the plasmalemma. Thus, their differential lipid composition is most likely the source of the distinct

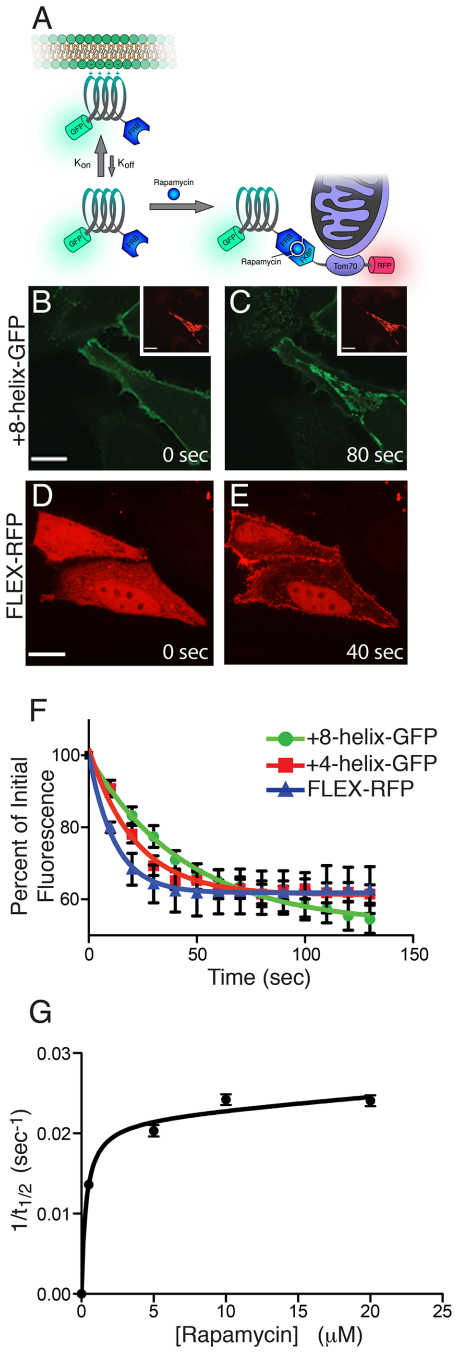

FIGURE 6: Measurement of probe dissociation rate using a rapamycin heterodimerization system. (A) Diagrammatic representation of the system used to assess the rate of dissociation of charge probes from the membrane. Surface charge probes tagged with GFP and an FRB domain were transfected into cells, along with RFP and FKBP-tagged Tom70 (FKBP-Tom70-RFP), which localizes to mitochondria. Because the charge probe interacts reversibly with the membrane, it can be recruited to mitochondria irreversibly upon addition of rapamycin. The rate of detachment from the membrane (K_{off}) is dictated by the membrane surface charge. (B, C) Confocal images of HeLa cells cotransfected with an FRB- and GFP-tagged +8 helical charge probe and FKBP-Tom70-RFP, before, B, and 80 s after addition of 10 μM rapamycin, C. (D, E) Confocal images of HeLa cells cotransfected with a soluble FRB- and RFP-tagged probe (FLEX-RFP) and a nonfluorescent plasma membrane–targeted FKBP-tagged construct (FKBP-Lyn), before, D, and 40 s after addition of 10 μM rapamycin, E. Images in B–E are representative of at least 15 cells from at least three different experiments for each condition. (F) Comparison of the rate of rapamycin-induced dissociation of FRB- and GFP-tagged +8 and +4 helical charge probes from the plasma membrane with the rate of disappearance of FLEX-RFP from the cytosol due to rapamycin-induced recruitment to the plasma membrane. Exponential decay curves were fitted using Prism software. (G) Quantification of the rate of dissociation of the FRB- and GFP-tagged +8 helical charge probe from the membrane as a function of the concentration of rapamycin added to induce its recruitment to mitochondria. The inverse of the $t_{1/2}$ for recruitment (in s^{-1}) is plotted vs. the concentration of rapamycin. Data are means ± SE of three independent experiments and the curve was fitted to a one-site saturable binding model using Prism

surface charge of the organelles. This contrasts sharply with the exofacial aspect of the plasmalemma, where surface charge is dictated largely by anionic carbohydrates. Indeed, treatment of cells with neuraminidase collapses the ζ potential of intact cells (Luner *et al.*, 1975; Silva Filho *et al.*, 1987).

We also attempted to estimate the surface potential of the inner leaflet of the plasma membrane by comparison with pure lipid liposomes of known ζ potential. To this end, we measured the rate of dissociation of charged probes, a parameter that is independent of their level of expression. Giant liposomes were used to mimic the curvature of the cellular membrane. By comparing the dissociation rates in intact cells with those measured in liposomes of varying composition we concluded that the potential of the plasma membrane is equivalent to that of a bilayer consisting of 14% monovalent anionic lipid (PtdSer). This value is lower than predicted from the reported composition of the plasma membrane, which is thought to contain 10–15% PtdSer, plus 1–2% each of PtdIns(4)P and PtdIns(4,5)P_2 and much smaller amounts of PtdIns(3,4,5)P_3. The additional presence of PtdIns, which was earlier taken for granted (e.g., van Meer *et al.*, 2008), is currently under debate. Because virtually all the PtdSer of the plasma membrane resides in its cytosolic monolayer, the total content of anionic lipids therefore exceeds that estimated above. The apparent discrepancy can be readily explained by the presence of cationic proteins that, by adhering to the membrane surface, mask its net charge. Accordingly, a variety of soluble polycationic, often amphiphilic proteins including—but not limited to—MARCKS, K-Ras, c-Src, and Rac-1 bind constitutively to the plasma membrane, effectively neutralizing its net charge (McLaughlin, 1989; McLaughlin *et al.*, 2002). In addition, the cytosolic tails of many transmembrane proteins contain polycationic stretches that are tightly apposed to the negative head-groups of anionic phospholipids (McLaughlin *et al.*, 2002). Thus, our measurements likely reflect the net, effective surface charge of the membrane.

It is worth emphasizing that these determinations provide only a macroscopic, stationary estimate of the surface potential of a resting cell. The methods we used are diffraction-limited and cannot discern differences between membrane nanodomains. Moreover, it is well established that acute changes in lipid composition can occur during events such as phagocytosis, macropinocytosis, and apoptosis, or when cytosolic calcium is elevated in response to stimulation. These conditions are expected to alter the surface charge and hence the electrostatic interaction of proteins with the membrane. Conversely, phosphorylation of cationic proteins like MARCKS alters their ability to associate with the membrane. This not only causes relocalization of the phosphorylated proteins, but also may affect other molecules by unmasking charges in the membrane. Clearly, more dynamic methods with higher resolution will be required in the future to better assess the electrostatic properties of biological membranes.

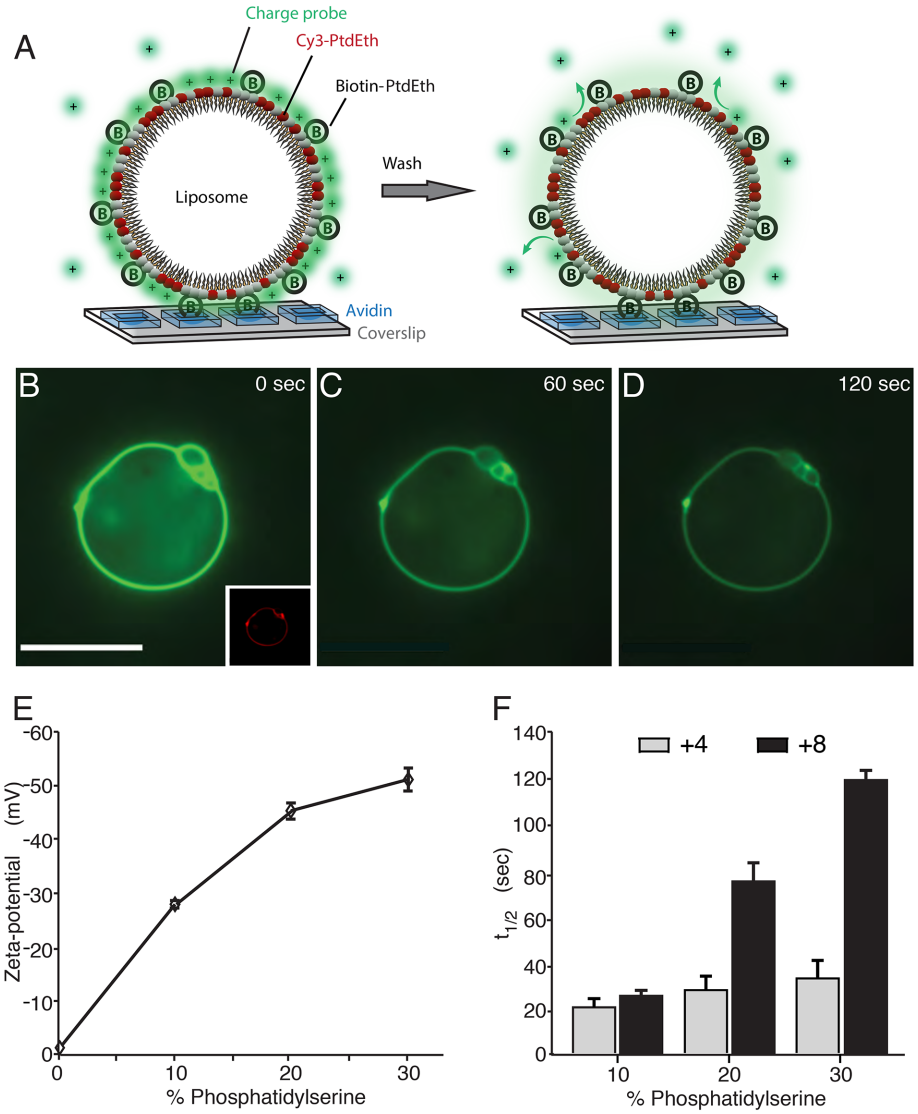

FIGURE 7: Measurement of the dissociation rate of the +8 charge probe from artificial liposomes and its relationship to the zeta potential. (A) Diagrammatic representation of the procedure used to measure the rate of dissociation of the +8 helical charge probe from GUVs. GUVs were generated using varying ratios of PtdCho and PtdSer, containing in addition Cy3-labeled PtdEth to enable visualization by fluorescence microscopy and biotinylated PtdEth to facilitate their attachment to avidin-coated coverslips. The GUVs were allowed to equilibrate with the green fluorescent charge probe and dissociation was initiated by washing the probe off with a large volume of medium. Repeated image acquisition was used to assess the rate of dissociation, ensuring that photobleaching was negligible. (B–D) Dissociation of FITC-labeled +8-helical synthetic peptide from a GUV containing 20% PtdSer. (B) Image of the GUV equilibrated with 50 ng/ml in the labeled probe. The outline of the GUV, visualized as the emission of Cy3-PtdEth, is shown in the inset. (C, D) Images acquired 60 s, C, and 120 s, D, after the unbound probe was washed. Images are representative of 15 similar determinations. (E) Zeta potential measurements of liposomes containing 0, 10, 20, and 30% PtdSer. (F) $t_{1/2}$ of the dissociation rate of +8-helical (black bars) and +4-helical synthetic (gray bars) probes from GUVs containing 10, 20 and 30% PtdSer. Data are means ± SE of at least 15 similar determinations for each condition.

MATERIALS AND METHODS

Reagents

Rapamycin, ultralow–gelling temperature agarose, 1,2-dioleoyl-*sn*-glycero-3-phosphoethanolamine-N-(cap biotinyl), and streptavidin from *Streptomyces avidinii* were from Sigma-Aldrich (Oakville, Canada). FM4-64, tetramethylrhodamine-conjugated concanavalin A (TMR-Con A), and Alexa 647-conjugated avidin were from Invitrogen Molecular Probes. POPtdSer, DOPtdCho, biotin-PtdEth, and rhodamine-PtdEth were from Avanti Polar Lipids (Alabaster, AL). The FITC-labeled NH_2-SKLKRLFKRLRKWFKKG-C-COOH (FITC-+8) and NH_2-SALAALFARLRKWFKKG-C-COOH (FITC-+4) peptides were synthesized by Bio-Synthesis (Lewisville, TX).

Cell culture

RAW264.7 murine macrophages and HeLa cells were obtained from the American Type Culture Collection (Manassas, VA) and grown in medium RPMI 1640 and DMEM, respectively, supplemented with 10% heat-inactivated fetal bovine serum at 37°C under 5% CO_2.

Plasmids

The following plasmids were used in this study: +2-Pre-GFP, +4-Pre-GFP, +6-Pre-GFP, +8-Pre-GFP, +2-helix-GFP, +4-helix-GFP, +6-helix-GFP, +8-helix-GFP, and PM-RFP (Yeung *et al.*, 2006); iRap-GFP-+8-helix, iRap-GFP-+6-helix, iRap-GFP-+4-helix, FKBP-Tom70-RFP (Silvius *et al.*, 2006); mRFP-FKBP (Szentpetery *et al.*, 2010); mCh-Sec61-β was from Addgene (plasmid 49155); RFP-sialyl-transferase was a kind gift of E. Rodriguez Boulan; RFP-UBSKL was a gift from P. K. Kim; RFP-LAMP was from Addgene (plasmid 1817).

Transient transfection

RAW 264.7 or HeLa cells were plated onto 1.8-cm glass coverslips and allowed to reach 60–80% confluency. The cells were then transfected with the indicated plasmid(s) using FuGENE HD (RAW 264.7 cells) or FuGENE 6 (HeLa cells; Promega, Madison, WI) according to the manufacturer's instructions. Briefly, 0.5 µg of plasmid DNA and 1.5 µl of transfection reagent were mixed into 100 µl of serum-free medium, preincubated for 15 min, and then added to the cells. Experiments were typically initiated 24 h after transfection.

Permeabilization, endomembrane labeling, and resealing

For permeabilization, RAW264.7 cells were grown on coverslips as above, washed with HEPES-buffered RPMI then incubated at 37°C in 500 µl loading buffer (70 mM KCl, 70 mM K-glutamate, 5 mM ATP, 1 mM EGTA, 1 mM DTT, 10 mM HEPES, pH 7.4) containing 2 µg/ml FM4-64 for 30 s, then resealed by washing twice with recovery buffer (70 mM KCl, 70 mM K-glutamate, 1 mM $MgCl_2$, 1 mM DTT, 10 mM HEPES, pH 7.4). FM4-64 fluorescence was visualized with excitation at 514 nm and emission at 640 nm to enable simultaneous visualization of green and red fluorescent proteins.

	$z = 4$	$z = 6$	$z = 8$	Average surface potential[a]
ER	17.29 ± 0.82	16.92 ± 0.42	27.48 ± 2.38	–14.4 mV
Mitochondria	8.18 ± 0.81	12.57 ± 0.57	19.55 ± 1.48	–21.5 mV
Golgi	17.48 ± 1.17	13.72 ± 0.78	13.91 ± 1.11	–20.0 mV
Plasma membrane			–35.0 mV	

[a]Rightmost column shows the calculated (absolute) average surface potential.

TABLE 1: Computed surface potentials (in mV) of organelles relative to that of the plasma membrane as determined by Eq. 4 (see Appendix).

Rapamycin induction

Cells were plated on coverslip and transfected as described above with the indicated iRap-GFP-charge probe and FKBP-Tom70-RFP. Twenty-four h after transfection, cells were imaged by confocal fluorescence microscopy before and at the indicated times after rapamycin addition (5, 10, and 20 μM).

Giant liposome formation

Giant unilamellar vesicles (GUVs) were prepared as described by Horger *et al.* (2009). Briefly, 6.2 mM lipids (PtdCho, PtdSer, rhodamine-PtdEth) containing 1% of either biotin-PtdEth or 1,2-dioleoyl-*sn*-glycero-3-phosphoethanolamine-N-(cap biotinyl) were spread on a glass slide covered with 1% ultralow–gelling temperature agarose, incubated for 3 h in phosphate-buffered saline (PBS) at 37°C, and then placed on a coverslip coated with Alexa647-avidin or streptavidin (25 μg/ml) to allow binding of the biotinylated GUVs to avidin for 5 min. The FITC-+8 or FITC-+4 peptides were then added and the GUVs were imaged by fluorescence microscopy before and at increasing times after the peptides were removed from the medium.

Zeta potential measurements

Liposomes were prepared as describe earlier (Roy *et al.*, 2000). Briefly, lipids were dried under nitrogen, resuspended in 1 ml 10 mM Tris, sonicated in a bath sonicator, and then passed through a liposome extruder using 10-nm and 1000 nm-filters, as indicated. ζ potential was measured using the Zetasizer Nano ZS (Malvern).

Microscopy

For imaging, cells grown on coverslips were mounted in a Chamlide magnetic chamber (Seoul, South Korea), overlaid with 1 ml of medium (PBS for experiments using rapamycin or involving GUVs; recovery buffer for other cellular experiments). For experiments involving rapamycin or GUVs, fluorescence microscopy was performed using a spinning-disk confocal system (Quorum Technologies, Guelph, Canada). Our system is based on an Axiovert 200M microscope (Carl Zeiss) equipped with a 63× oil-immersion objective (numerical aperture 1.4) and a 1.5×-magnifying lens. The microscopes carry a motorized XY stage (Applied Scientific Instrumentation, Eugene, OR), a Piezo Z-focus drive, and diode-pumped solid-state lasers emitting at 440, 491, 561, 638, and 655 nm (Spectral Applied Research, Richmond Hill, Canada). Images were recorded with a back-thinned cooled charge-coupled device camera (Hamamatsu Photonics) under command of the Volocity software (version 6.2.1; PerkinElmer, Woodbridge, Canada). Selection of regions of interest and fluorescence intensity measurements were performed with ImageJ (version 1.48; National Institute of Health, Bethesda, MD). When brightness and contrast adjustments were performed, the parameters were adjusted across entire images without altering the linearity of mapped pixel values. Time-lapse images are representative of at least 10 cells each from four separate experiments.

All other imaging of live cells was performed using a Leica TCS SP8 laser scanning confocal microscope equipped with a white-light laser (470–670 nm), an argon laser (458/476/488/496/514 nm), and a 405-nm laser, using a 63× objective with 1.4 N.A. Images were acquired with HyD detectors under the command of the Leica LAS software. Images were deconvolved, and then selection of regions of interest and measurements of fluorescence intensity were performed with Volocity software (version 6.2.1; PerkinElmer, Woodbridge, Canada).

ACKNOWLEDGMENTS

We thank John Silvius for his expert advice and his generous gift of plasmids. This work was supported by Foundation Grant FDN-143202 from the Canadian Institutes of Health Research to S.G.

REFERENCES

Bolte S, Talbot C, Boutte Y, Catrice O, Read ND, Satiat-Jeunemaitre B (2004). FM-dyes as experimental probes for dissecting vesicle trafficking in living plant cells. J Microsc 214, 159–173.

Dubyak GR (2007). Go it alone no more—P2X7 joins the society of heteromeric ATP-gated receptor channels. Mol Pharmacol 72, 1402–1405.

Ferreira L, Pereira L, Faria R (2015). Fluorescent dyes as a reliable tool in P2X7 receptor-associated pore studies. J Bioenerg Biomembr 47, 283–307.

Hammond GR, Machner MP, Balla T (2014). A novel probe for phosphatidylinositol 4-phosphate reveals multiple pools beyond the Golgi. J Cell Biol 205, 113–126.

Hasegawa J, Strunk BS, Weisman LS (2017). PI5P and PI(3,5)P_2: minor, but essential phosphoinositides. Cell Struct Funct 42, 49–60.

Horger KS, Estes DJ, Capone R, Mayer M (2009). Films of agarose enable rapid formation of giant liposomes in solutions of physiologic ionic strength. J Am Chem Soc 131, 1810–1819.

Leventis PA, Grinstein S (2010). The distribution and function of phosphatidylserine in cellular membranes. Annu Rev Biophys 39, 407–427.

Luner SJ, Sturgeon P, Szklarek D, McQuiston DT (1975). Effects of proteases and neuraminidase on RBC surface charge and agglutination. Vox Sang 28, 184–199.

McLaughlin S (1989). The electrostatic properties of membranes. Annu Rev Biophys Biophys Chem 18, 113–136.

McLaughlin S, Wang J, Gambhir A, Murray D (2002). PIP_2 and proteins: interactions, organization, and information flow. Annu Rev Biophys Biomol Struct 31, 151–175.

Olivotto M, Arcangeli A, Carlà M, Wanke E (1996). Electric fields at the plasma membrane level: a neglected element in the mechanisms of cell signalling. Bioessays 18, 495–504.

Quatela SE, Sung PJ, Ahearn IM, Bivona TG, Philips MR (2008). Analysis of K-Ras phosphorylation, translocation, and induction of apoptosis. Methods Enzymol 439, 87–102.

Roy MT, Gallardo M, Estelrich J (1998). Influence of size on electrokinetic behavior of phosphatidylserine and phosphatidylethanolamine lipid vesicles. J Colloid Interface Sci 206, 512–517.

Roy MO, Leventis R, Silvius JR (2000). Mutational and biochemical analysis of plasma membrane targeting mediated by the farnesylated, polybasic carboxy terminus of K-ras4B. Biochemistry 39, 8298–8307.

Silva Filho FC, Santos AB, de Carvalho TM, de Souza W (1987). Surface charge of resident, elicited, and activated mouse peritoneal macrophages. J Leukoc Biol 41, 143–149.

Silvius JR (1999). Fluorescence measurement of lipid-binding affinity and interbilayer transfer of bimane-labeled lipidated peptides. Methods Mol Biol 116, 177–186.

Silvius JR, Bhagatji P, Leventis R, Terrone D (2006). K-ras4B and prenylated proteins lacking "second signals" associate dynamically with cellular membranes. Mol Biol Cell 17, 192–202.

Szentpetery Z, Várnai P, Balla T (2010). Acute manipulation of Golgi phosphoinositides to assess their importance in cellular trafficking and signaling. Proc Natl Acad Sci USA 107, 8225–8230.

Tippe A (1981). Electrophoretic measurements about the relation between transition voltage and zeta-potential of biological membranes. Biochim Biophys Acta 641, 395–400.

van Meer G, Voelker DR, Feigenson GW (2008). Membrane lipids: where they are and how they behave. Nat Rev Mol Cell Biol 9, 112–124.

Vandrangi P, Jreij P, Rajapaksa TE, Bansal N, Lo DD, Rodgers VG (2012). Novel in situ normal streaming potential device for characterizing electrostatic properties of confluent cells. Rev Sci Instrum 83, 074302.

Wright LP, Philips MR (2006). Lipid posttranslational modifications. CAAX modification and membrane targeting of Ras. J Lipid Res 47, 883–891.

Yeung T, Terebiznik M, Yu L, Silvius J, Abidi WM, Philips M, Levine T, Kapus A, Grinstein S (2006). Receptor activation alters inner surface potential during phagocytosis. Science 313, 347–351.

Yeung T, Gilbert GE, Shi J, Silvius J, Kapus A, Grinstein S (2008). Membrane phosphatidylserine regulates surface charge and protein localization. Science 319, 210–213.